01

# Thermal-field emission in nanostructures with resonant tunneling

© M.V. Davidovich

Saratov National Research State University,
410012 Saratov, Russia
e-mail: davidovichmv@info.sgu.ru

Received July 6, 2023
Revised October 15, 2023
Accepted October 18, 2023

A model of thermal field emission in nanostructures with several barriers and potential wells between them is presented, based on a strict definition of the shape of the quantum potential and a strict solution of the Schrodinger equation, taking into account the thermal balance and the influence of spatial charge. Vacuum and semiconductor resonant tunneling diode and triode structures with two, three or more electrodes are considered. A formula is given for correcting the quantum potential due to the influence of spatial charge. In general, it is necessary to consider two-way tunneling and heating of electrodes with different temperatures due to current flow. Conditions are considered when the contribution of the reverse current is small, when thermal current or tunnel current can be neglected. The approach can be extended to the non-stationary case.

**Keywords:** resonant tunneling, thermal-field emission, vacuum nanotriode, potential barrier, quantum well.

DOI: 10.61011/JTF.2024.01.56899.170-23

## Introduction

An emission current is generated when external fields are applied to conductors. The thermoelectronic emission [1–3] and field (autoelectronic) emission [1,4–8] are usually considered separately. The second type of emission is characterized by the fact that the temperature in the Fermi–Dirac (FD) distribution

$$f_{\mathrm{FD}} = \left[1 + \exp\left((E - \mu_c)/(k_{\mathrm{B}}T)\right)\right]^{-1}$$

is assumed to be zero. This works well up to room temperatures of $k_{\mathrm{B}}T \sim 0.026$ eV. The current density from the cathode to the anode with the anode voltage $U_a$ in this approximation is

$$J^+(U_a) = \frac{-em_e}{2\pi^2\hbar^3}\int_0^{\mu_c} D^+(E, U_a)(\mu_c - E)dE. \qquad (1)$$

Next, all values corresponding to the cathode are denoted by the index „$c$“, the values corresponding to the anode are denoted by the index „$a$“, the values corresponding to the grid are denoted by the index „$g$“. There is consistency between the concepts of cathode and source, as well as anode and drain in case of solid-state nanostructures. Thermal emission is characterized by relatively small fields and high (on the order of 1000–2000 K) temperatures. A number of papers [8–20] addressed the general thermal-field emission, but only from the cathode, while the shape of the potential function and the strict solution of the Schrodinger equation (SE), as a rule, were not taken into account. Taking this into account is important for nanostructures, and it is also important to address the two-way tunneling and different temperatures of the cathode and anode, which is the purpose of this study. Moreover, the impact of the spatial charge on the change in the quantum potential is important, which is not considered in this paper. Taking into account thermal field emission is also important for emitters with points [18–21], for which the heating can be strong, heterogeneous and may lead to explosive emission.

We will consider diode structures, as well as triode structures (Fig. 1) with single or double grids at the same grid electrostatic potential $U_g$ and quantum potential $V_g = -eU_g + E_{Fc}$. Accordingly, for the anode $V_a = -eU_a + E_{Fc}$. Formally, it can be assumed that the Fermi energy (FE) slightly increases at room temperature because of thermal broadening from $E_{Fc} = \mu_c$ to $E_{Fc} = \mu_c + k_{\mathrm{B}}T$, and then current density can be

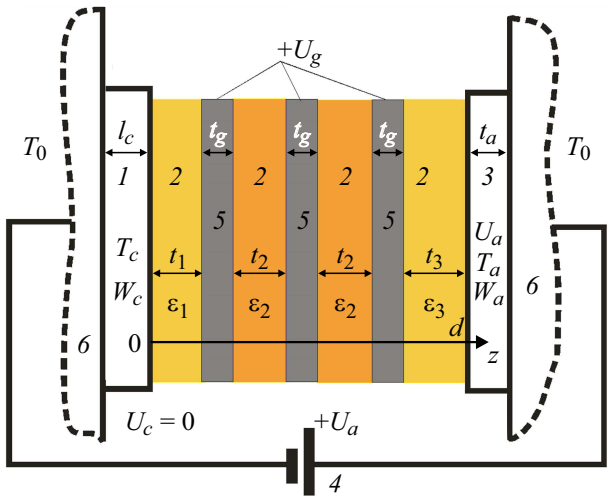


**Figure 1.** Resonant tunnelling structure circuit in the form of a cathode *1*, dielectric layers *2*, anode *3*, power supply *4*, grid electrodes *5* and thermostats *6*.

determined as

$$J^+(U_a) = \frac{-em_e}{2\pi^2\hbar^3}\int\limits_0^{\mu_e+k_BT} D^+(E,U_a)(\mu_c + k_BT - E)dE.$$

The current density from the anode to the cathode is given by the same (1) formula

$$J^-(U_a) = \frac{-em_e}{2\pi^2\hbar^3}\int\limits_0^{\mu_a} D^-(E,U_a)(\mu_a - E)dE. \qquad (2)$$

The electrochemical potentials $\mu_c = E_{Fc}$, $\mu_a = E_{Fc} - eU_a$ and penetrability $D^{\pm}$ are introduced into the formulas. The total current density is $J(U_a) = J^+(U_a) - J^-(U_a)$. The charge of the electron here is $q_e = -e$, and its mass is $m_e$. We have $J^-(U_a) = 0$ at $eU_a \geq E_{Fa}$, since there are no levels at the cathode for tunneling electrons from the anode. In this case, it is convenient to count the energy from the bottom of the cathode conduction band. Some electrons can tunnel from the anode at $eU_a < E_{Fa}$, and in this case it is convenient to count energy from the lower bottom of the anode conduction band. The energy of the electrons at the cathode increases by $eU_a$. The energy is counted from the bottom of the cathode conduction band in ratios (1), (2), the values $D^+(E,U_a)$ and $D^-(E,U_a)$ characterize the penetrability (transmittance) of the barrier. Further, barrier means any distribution of the quantum potential $V(x)$ included in the SE. At $eU_a \geq 1$ the eV barrier is strongly asymmetric, and it can be assumed that $|D^+(E,U_a)| \gg |D^-(E,U_a)|$. In this case, the total current density is $J(U_a) \approx J^+(U_a)$. In the case of an arbitrary temperature, the density of electrons with energy $E = p_z^2/(2m_e) = m_e v_z^2/2$ incident per second per unit cathode surface at $z = 0$ is ([1], formula 4.27)

$$dn_E^+ = \frac{m_e k_B T}{2\pi^2\hbar^3}\ln\left(1 + \exp\left(\frac{\mu_c - E}{k_BT}\right)\right)dE = A(E)dE. \qquad (3)$$

This formula is obtained taking into account the distribution of FD and integration over all contributions $(p_x^2 + p_y^2)/(2m_e)$, corresponding to the transverse pulses of incoming electrons. The chemical potential at the cathode is FE in (3): $\mu_c = E_{Fc}$. $\mu_c \to \mu_a = E_{Fa} - eU_a$ needs to be replaced on anode in distribution (3). Using (3), we obtain $J(U_a, T_c, T_a) = J^+(U_a, T_c) - J^-(U_a, T_a)$ and

$$J^+(U_a,T_c) = \frac{-em_e k_B T_c}{2\pi^2\hbar^3}\int\limits_0^{\infty} D^+(E,U_a) \times \ln\left(1 + \exp\left(\frac{\mu_c - E}{k_BT_c}\right)\right)dE, \qquad (4)$$

$$J^-(U_a,T_a) = \frac{-em_e k_B T_a}{2\pi^2\hbar^3}\int\limits_0^{\infty} D^-(E,U_a) \times \ln\left(1 + \exp\left(\frac{\mu_a - E}{k_BT_a}\right)\right)dE. \qquad (5)$$

These are the basic equations of thermal field emission (TFE). Obviously, we obtain (1) and (2) from them with $T_{c,a} \to 0$. Thermal emission is obtained in the approximation $k_BT_c \sim 0.2$ eV, $E \geq E_{Fc} + W_c$, $T_a = 0$ and $D^+(E,U_a) = 1 - |\tilde{R}|^2 \approx 1$. Here $|\tilde{R}|^2$ — the average power reflection coefficient from the over-barrier passage. At the same time, field emission (area $0 < E < E_{Fc} + W_c$) is ignored, since $D^+(E,U_a) \ll 1$ at low voltages. $eU_a \ll W_c$ is required for this purpose, i.e. $eU_q \sim k_BT_c$. In this case, the accelerating electrode is usually located far enough away, so that the resulting barrier is wide enough and almost rectangular with a height of $W_c$ above the Fermi level (FL) $E_{Fc}$. The coefficient $\tilde{R}$ is located as a reflection from the step $W_c$ when passing over it. The current density in this approximation is given by the Richardson equation $J_T = -A_0T^2\exp\left(-W_c/(k_BT_c)\right)$, where $A_0 = 2^5\pi^4 m_e e k_B^2/\hbar^3$ — Sommerfeld thermoelectronic constant. It should be noted that if for field emission in (1) we put $D^+ = 1$ for all energies, then for the maximum density at $W_c = 4$ eV, $E_F = 14.6$ (beryllium) we have (at $T = 1500$ K)

$$\frac{J_{\max}}{J_T} = \frac{E_{Fc}^2}{2^7\pi^6(k_BT)^2}\exp\left(\frac{W_c}{k_BT_c}\right) \approx 4\cdot 10^7.$$

The maximum unattainable current density $10^{15}-10^{16}$ A/m$^2$ is given by the expression $J_{\max} = em_eE_{F_c}^2/(4\pi^2\hbar^3)$ [1] and corresponds to the hypothetical case when all outgoing electrons pass the barrier. It is unattainable due to its quantum properties. Theoretically, a current density of 2–3 of the order lower than [22,23] is achievable in resonant tunneling (RT) nanostructures, since the condition of full transmission is achieved for some energies. The electrodes are strongly heated due to the release of Joule heat at such a current density. The cathode is also heated due to the Nottingham effect. its contribution is significant at RT from levels significantly below FL. The anode is heated by Joule heat and the release of energy $eU_a$ by each electron. The cathode is cooled due to thermal emission. Therefore, high-precision RT nanostructures are characterized by the fact that the cathode and anode temperatures can be different and quite large, i.e. TFE should be taken into account. This is especially typical for vacuum resonant tunneling structures (RTS). In this respect, quantum RT nanostructures are very different from incandescent thermal cathodes with TFE, because their temperatures are determined by the processes of current flow, i.e. they can vary in time and space. Moreover, the use of incandescent cathodes implies that the anode is cold (heat is released in the collector), and the anode voltage is high enough, so that emission from the cathode is considered only. Fig. 1 shows a typical RT nanostructure. The dielectric layers *2* in RT nanostructure can be made of various dielectrics, or RT nanostructures may have no dielectic layers. CVD (chemical vapor deposition) diamond films with a high content of the diamond phase of carbon ($sp^3$-hybridized atoms) are the most suitable [24]. Films

in the form of graphite nanoclusters can be deposited as conductive layers, *n*-layered graphene or other conductive films can be used. Heterostructures based on GaAs technology are most often used for RT diodes and quantum cascade lasers — $Ga_xAl_{1-x}As$. The RT structure (Fig. 1) corresponds to three quantum wells of the same depth. It is possible to consider RTS with one, two and three wells. It is necessary to increase the electron free path length (FPL) since RT needs ballistic transport in case of a large number of layers, which requires the reduction of the temperature. It is difficult to use cryogenic temperatures, therefore, it is really possible to obtain from three to seven layers if the length of the entire structure does not exceed 10 nm.

The purpose of this work is the calculation of TFE at arbitrary temperatures of the cathode $T_c$ and the anode $T_a$ in nanostructures with dielectric and conductive layers, as well as in the case of vacuum gaps between grids using an accurate quantum potential and based on an accurate solution of SE. The aim is also to obtain a thermal balance and estimate the temperature of the electrodes in a high-current density RTS. We use a number of approximations since this task is very difficult for nanostructures, especially in terms of thermal conductivity [25–33]. The basic assumption is equilibrium and stationarity. The temperature distribution is sought within the framework of this model. The second assumption is that the size of the transit section „cathode boundary−anode boundary“ (Fig. 1) is less than the free path length. This is the main requirement for emission electronics supporting ballistic transport. There is no heat release in this region, and it all occurs on the electrodes — anode and cathode at their free path lengths (i.e. at lengths of the order of tens of nanometers). The size of the cathode and anode is significantly larger — several hundred nanometers, i.e. there is diffusion transport, and there is heat release in the form of Joule heat. Such relatively small sizes of the cathode and anode are taken for increasing the temperature gradient and increasing the outflow of heat into the thermostats. This made it possible to use a linear temperature distribution and obtain relatively low temperatures at high current densities. In reality, such a linear temperature is determined at lengths of the order of several free path lengths. Fourier's law may be somewhat violated with such large gradients, i.e., the heat flow may depend on temperature and size, as well as be proportional to some degree of temperature. Nevertheless, we consider phonon transport to be diffusive, consider the linear equation of thermal conductivity and use tabular values of thermal conductivity coefficients. This suggests that the results obtained should be considered qualitative. Otherwise, it would be necessary to solve the heat equation taking into account nonlinear effects, if necessary, to determine the parameters included in it, and the heat balance model would be very complex and difficult to solve.

The cases of a triode with one and two grids, as well as the case of a diode, are considered. RTS may contain vacuum gaps instead of dielectric layers in a special case. There is no ballistic thermal conductivity in this case. It should be noted that there are a number of works where the TFE is considered to one degree or another [8–20]. In particular, the emission from points is considered [19,20]. However, the general equations (4), (5) were not considered for bilateral emission. The quantum potential with the exact solution of SE was also not accurately taken into account. The application of the formula (4) is considered in [11] (see also [12–16]), i.e. it was believed that $D^-(E, U_a) = 0$. However, the formula (5) should be taken into account for RTS, in the case when the resonant level falls into the region of electron energies at the anode and $D^-(E, U_a) = 1$. This does not take place if $eU_a > E_{Fc}$ and the anode temperature is close to zero. However, there are electrons of all energies on it at the final temperature of the anode. Moreover, (5) should be taken into account in structures with low anode voltage, which can be realized in solid-state heterostructures used in RT diodes and transistors.

## 1. Thermal balance in quantum heterostructures

Thermal emission uses heated incandescent cathodes at relatively low anode voltages, when field emission can be ignored. These voltages are such that the field at the cathode is significantly lower than $10^7$ V/cm — the threshold level when field emission (FE) begins to manifest itself. These voltages are on the order of fractions of V in case of nanoscale structures. Further beam acceleration is achieved by a second anode in the case of electron guns. High current densities can be achieved in case of FE, at which significant cathode heating occurs resulting in TFE. High tunnel current densities are typical for RTS. An additional strong cathode heating occurs due to the Nottingham effect in case of tunneling through resonant levels well below FL. This requires taking into account TFE. RTS with two, three or more electrodes (Fig. 1) are currently among the most promising for the development of high-frequency electromagnetic ranges, including THz and IR ranges jcite33-48, and also as FE high-current sources [22,23]. At the same time, it is necessary to consider RT for the analysis of resonant tunneling diodes, transistors, quantum cascade lasers on the Stark ladder and similar structures. The specific feature of RT is an increase of the emission current by several orders of magnitude compared with tunneling through a single barrier. A single barrier is typical for a conventional diode structure with a vacuum in the cathode−anode space, or when this space is filled with a homogeneous dielectric. In the latter case, the barrier decreases by $\varepsilon$ times at a multiple of dielectric permittivity (DP). Such a decrease of the barrier can also result in an increase of current by several orders of magnitude. It is necessary to consistently solve the SE, Poisson's equation (PE) and Fourier thermal conductivity equation for strict modeling of RTS in the case of a high current density (and, accordingly, a spatial charge). Fourier thermal conductivity

equation may be omitted for nanostructures because of the ballistic transport of phonons. The thermal conductivity coefficient is usually changed in this case. The radiation heat transfer should be taken into account in RTS with vacuum gaps at high electrode temperatures. The thermophysics of nanostructures is very complex [25–32]. Estimates show a small contribution of radiative heat transfer, especially in case of close cathode and anode temperatures, which is quite possible in case of usage of approximate estimates (see table). Further, we do not consider heat release in layers, since the transport of electrons and phonons is almost ballistic, and the corresponding heat release occurs on the FPL of electrons and phonons at the cathode and anode. Heat is released on the electron FPL from the Nottingham effect, as well as from hot electrons hitting the anode. The Nottingham effect heats up the electron-emitting electrode, while the thermal radiation of the electrons cools them. Therefore, the thermal balance is very difficult even in steady-state mode, when the surface temperatures of the electrodes are determined. In reality, the temperature distribution in nanostructures should be considered. We will consider nanostructures (Fig. 1) located on massive thermostats at room temperature $T_0$, while for simplicity we assume that the temperatures of the cathode and anode are distributed linearly depending on the coordinate $x$. In this case, there is no need to solve the Fourier thermal conductivity equation, and it is very easy to obtain a thermal balance, as well as a temperature distribution. The most common case are really linear or close to linear temperature distributions. Next, we consider the transverse dimensions to be significantly superior to the longitudinal ones, i.e. we use one-dimensional equations. These one-dimensional equations can be written respectively as follows in the case of one-dimensional stationary tunneling

$$\left(-\frac{\hbar^2\partial_x^2}{2m_e}+V(x)-E\right)\Psi(x,E,T)=0, \tag{6}$$

$$\partial_x^2 U(z)=\frac{e|\Psi(x,E,T)|^2}{\varepsilon_0\varepsilon(z)}, \tag{7}$$

Dependence of cathode surface temperatures $T_c$ and anode $T_a$ on length $l=l_c=l_a$ nm (electrode material — copper, $T_0=300$ K)

| Density current $J$, A/m$^2$ | Temperature-tour, K | Length $l$, nm | | | | | |
|---|---|---|---|---|---|---|---|
| | | 80 | 160 | 240 | 320 | 400 | 480 |
| $7.5\cdot10^{11}$ | $T_c$ | 551 | 834 | 1150 | 1498 | 1879 | 2292 |
| | $T_a$ | 668 | 1070 | 1504 | 1970 | 2468 | 2999 |
| $5.2\cdot10^{11}$ | $T_c$ | 570 | 856 | 1157 | 1474 | 1805 | 2152 |
| | $T_a$ | 475 | 666 | 872 | 1093 | 1329 | 1581 |
| $8.1\cdot10^{11}$ | $T_c$ | 731 | 1199 | 1703 | 2244 | 2822 | 3436 |
| | $T_a$ | 562 | 862 | 1198 | 1570 | 1978 | 2425 |

$$-\alpha^2(x)\partial_z^2(T)(x)=-\left(\frac{\kappa(x)}{c_p(x)\rho(x)}\right)\partial_x^2T(x)=f(x,T)$$
$$=\frac{F(x,T)}{c_p(x)\rho_m(x)}. \tag{8}$$

Here, the electrostatic potential $U$ is related to the quantum potential $V$ by the ratio $V(x)=V_0(x)-eU(x)-exU_a/d$, where $V_0(x)$ is the part of the quantum potential associated with the action of the structure (electrodes) during the movement of a point electron, $-eU(x)$part of the quantum potential associated with the action of spatial charge on this electron, and $-exU_a/d$ part of the quantum potential associated with the electrostatic potential in the cathode–anode flat structure. The potential $V_0(x)$ is based on multiple images. The singular term associated with the divergence of the Green's function (GF) is thrown out of it, since the electron does not act on itself. Essentially, $V_0(x)$ (with precision up to multiplier) is an electrostatic GF of an electron in a structure with a removed singular part. Its form is shown below. We wrote the Fourier thermal conductivity equation (8) in a non-stationary form, since the temperature during tunneling can be a slow function of time. The following coefficients are introduced in it: $\alpha$ — thermometric conductivity coefficient, $\kappa(x)$ — thermal conductivity coefficient, $c_p(x)$ — heat capacity coefficient at constant pressure, $\rho(x)$ — density coefficient. Further, for simplicity, we will assume that all coefficients are constant (at least piecewise constant). Stationary (steady-state) processes in the case of tunneling should actually be considered quasi-steady-state and slowly changing. Accordingly, in SE (6)

$$i\hbar\partial_t\Psi(x,t,T)=\hat{E}\Psi(x,t,T)=\left[V(x,t,T)-\hbar^2\partial_x^2/(2m_e)\right]$$
$$\times\Psi(x,t,T),$$

PE (7) is already stationary, not a wave equation (the term $\partial_t^2$ is omitted, and the vector potential is also not considered), since the potential changes very slowly in it, like in SE. The charge density $\rho_e=-e|\Psi(z,E,T)|^2$, generally speaking, slowly depends on time. If the operator $\partial_t$ is omitted in Fourier thermal conductivity equation, then slow thermal processes close to steady-state processes are considered. It is necessary to determine the density of thermal sources $F$ for solving the problem which strongly depends on the nature of tunneling. Therefore, each electron that tunnels from the level because of the Nottingham effect in case of RT, gives energy $E_{Fc}-E$ to the cathode region with a size of the order of FPL $\lambda$. We obtain the corresponding density of heat sources using (3).

$$F_N(E,T_c,U_a)=\frac{m_ek_BT_c}{2\pi^2\hbar^3\lambda}D^+(E,U_a)(E_{Fc}-E)$$
$$\times\ln\left(1+\exp\left(\frac{\mu_c-E}{k_BT_c}\right)\right)dE, \tag{9}$$

that is evenly distributed over the FPL in the region $-\lambda<x<0$. The total linear density should be obtained by

integrating and multiplying by the cathode cross-sectional area $S$, which is considered large for the 1$D$-model ($S \gg d^2$, $S \gg l_{c,a}^2$):

$$F_N(T_c, U_a) = S \int_0^{E_{Fc}} F_N(E, T_c, U_a) dE. \qquad (10)$$

Here $l_c$ and $l_a$ — the lengths of the cathode and anode, which for nanostructures are considered small (on the order of hundreds of nanometers), and the cathode and anode are considered to be located on massive thermostats at a temperature of $T_0$. Stationary solutions can be found in this case and the surface temperature of the cathode $T_c$ and the anode $T_a$ can be determined. The emission and thermal balance depend on them. The conduction current and tunnel current are continuous. We have a heat release density per unit cathode length due to Joule current heating

$$F_D(T_c, U_a) = \sigma^{-1} S J^2(T_c, U_a), \qquad (11)$$

where $\sigma$ — specific conductivity. Similar sources should be introduced at the anode. In addition, at $T_c > 0$ there are high-energy electrons $E > E_{Fc}$ that fall on the anode and give it energy $E + eU_a$ over a length of $\lambda$. Therefore

$$F_{Tc}(T_c, U_a) = \frac{m_e k_B T_c S}{2\pi^2 \hbar^3 \lambda} \int_{E_{Fc}}^{\infty} D^+(E, U_a)(E + eU_a) \times \ln\left(1 + \exp\left(\frac{\mu_c - E}{k_B T_c}\right)\right) dE. \qquad (12)$$

The ratio (3) is used in (12) and in (9). Sources attributable to the tunneling from the anode should also be considered. Thermal electrons passing over the barrier from the anode heat up the cathode, and the same electrons from the cathode cool it. These relations define a very complex nonlinear model, especially in the nonstationary case. The model can be simplified as follows. All parameters in (6)–(10) of the type of thermal conductivity, density, and specific conductivity coefficient are considered to be constant and not dependent of temperature. The model is considered to be stationary. We also consider $eU_a \geq E_{Fc}$, i.e. there is no RT from the anode, and the reverse current is small and can be neglected. We also consider a vacuum structure of size $d$, i.e. assume $\varepsilon = 1$. Only radiative heat transfer from the cathode to the anode is possible through vacuum gaps and it is usually small. Estimates show that it is small in case of a temperature difference of up to 1000 K. We neglect it. Ballistic transport of phonons is also possible. It is proportional to the temperature difference of the anode and cathode and helps to equalize these temperatures. It is necessary to know the appropriate effective coefficient of thermal conductivity for determination of ballistic transport of phonon and then it is quite simple to take it into account. Estimates show (see table) that the cathode and anode temperatures do not differ much, so this flux is small. This factoring is not necessary in case of the vacuum in the gaps between the grid electrodes. We assume that the cathode and anode are located on a massive thermostat with a temperature of $T_0$. This means that the area of the thermostat $S_0$ on which the cathode is stirred should satisfy the condition $S_0 \gg S$. In the case of solid-state RTS, we assume that the structure between the anode and cathode contains dielectric and metallic nanoscale layers (Fig. 1) with a total length of $d \ll \lambda$. This means ballistic electronic transport without heat generation and ballistic phonon heat transfer [26–33]. Accordingly, there is no grid current and heat dissipation on the grids. If we consider diamond layers, then their ballistic thermal conductivity is very high, as well as for thin carbon conductive layers. In this case, the temperature of the cathode and anode can be considered approximately the same, which simplifies the task. In this case, the thermal current from the cathode is greater than the thermal current from the anode because of the potential difference. Ballistic transport of electrons and phonons does not result in the heat release in the RTS [26–33]. High ballistic thermal conductivity results in an equalization of the temperatures of the cathode and anode surfaces, while the heat is generated because of the phonon transfer on an electrode with higher temperature. In this case it is necessary to use a grid material with an acoustic impedance close to the acoustic impedance of a diamond, i.e. reduce the Kapitza thermal resistance at the boundaries [25,26]. It is advisable to use nanoscale metal grids for this purpose. There is only radiation transfer from a hotter surface to a less hot surface in vacuum RTS with „weighted“ grids, and their temperatures may differ more strongly than for solid-state RTS. In this case, graphene-CNT grid structures are convenient [22].

For simplicity, it is convenient to assume that the temperature between the thermostats and the surfaces is distributed linearly. This distribution satisfies the Fourier thermal conductivity equation. It can be used for a simple calculation of the heat fluxes and determination of the heat balance. The best structures (Fig. 1) can be graphite or $n$-layered graphene electrodes separated by diamond layers. Crystalline diamond has a dielectric constant of $\varepsilon = 5.6$ and a very high thermal conductivity coefficient of $1001-2600\,\mathrm{W/(m \cdot K)}$. Therefore, the ballistic coefficient of thermal conductivity should be high. It is technologically convenient to produce heterostructures in the form of amorphous CVD diamond and well-conducting glass carbon or nanocrystalline graphite [49,50]. In the first case, the structure contains predominantly $sp^3$-hybridized carbon atoms, and in the second case it contains $sp^2$ carbon atoms. Polycrystalline diamond films produced by magnetron sputtering from low-pressure plasma can also be used. Anode cooling is possible in case of RT at anode levels ($eU_a < E_{Fc}$). The heat dissipation at the anode increases with an increase of the anode voltage, and the anode can be heated more strongly than the cathode. This will always be the case for a non-resonant diode structure

at high voltage. Electrons fly through the anode without scattering in case of field vacuum sources of electronic devices, and they are further accelerated by a second anode and are usually absorbed in a massive collector. If the cathode and anode are made of the same material, then each of the tunneling electrons releases energy $E_{Fc}-E$ at the cathode and gives energy $eU_a-E_{Fc}+E$ to the anode. If thermal electrons pass the barrier above FL, then the energy $E-E_{Fc}$ is taken away from the cathode, and these electrons cool the cathode. Also, both absorption and heat generation are possible at the anode. Note that these processes occur due to electrons entering or leaving the electrodes due to the conduction current, which is closed through the power supply. The conduction current is generated in the metal by electrons with FE. The electronic temperature at the cathode and at the anode is different, but with this movement, the temperatures equalize.

Let's consider the balance of thermal energy. Heat flow from the anode to the cathode $\kappa_d S(T_a-T_c)/d$. Here $\kappa_d$ — the diffusion coefficient of thermal conductivity. Heat flow from the cathode to the thermostat $\kappa_c S(T_c-T_0)/l_c$. Heat flow from the anode to the thermostat $\kappa_a S(T_a-T_0)/l_a$. The simplest model is obtained if we take the materials and lengths of the cathode $l_c$ and the anode $l_a$ the same. $\lambda = 39\,\text{nm}$ for copper at $T = 300\,\text{K}$. A large temperature gradient is created on such a nanoscale cathode, which contributes to the removal of heat into the thermostat. In reality, the lengths can be on the order of several FPL. We have the following for the balance at the cathode

$$\frac{\kappa_c(T_c-T_0)}{l_c} - \frac{\kappa_d(T_a-T_c)}{d} = \frac{F_N(T_c,U_a)+F_D(T_c,U_a)-F_{Tc}(T_c,U_a)}{S} = \tilde{F}_c(T_c,U_a). \tag{13}$$

Similarly for the balance on the anode

$$\frac{\kappa_a(T_a-T_0)}{l_a} + \frac{\kappa_d(T_a-T_c)}{d} = \frac{F_N(T_a,U_a)+F_D(T_a,U_a)-F_{Ta}(T_a,U_a)}{S} = \tilde{F}_a(T_a,U_a). \tag{14}$$

The right-hand sides (13) and (14) do not depend on $S$, and the equations themselves can be rearranged in the following form

$$T_c = \frac{T_0\kappa_c d + T_a\kappa_d l_c + \tilde{F}_c(T_c,U_a)l_c d}{\kappa_c d + \kappa_d l_c},$$

$$T_a = \frac{T_0\kappa_a d - T_c\kappa_d l_a + \tilde{F}_a(T_a,U_a)l_a d}{\kappa_a d + \kappa_d l_a}.$$

We will re-arrange these equations for several resonances as follows:

$$T_1 = T_0 + (l_1/k_1)\left[\sum_{n=1}^{N} D_n(E_{F1}-E_n)^2\,\frac{m_e}{2\pi^2\hbar^3}\,\Delta E_n + j^2\rho_1 l_1 - S(T_1,T_2)\right],$$

$$T_2 = T_0 + (l_2/k_2)\left[\sum_{n=1}^{N} D_n(E_1-E_{F2}+eU_a)\,\frac{m_e}{2\pi^2\hbar^3}\,\Delta E_n + j^2\rho_2 l_2 + S(T_1,T_2)\right].$$

$D_n = 1$ at full resonances, the permeability peaks at incomplete resonances are several orders of magnitude greater than its values between these peaks, which justifies the use of formulas. The electrode temperatures can be determined from these nonlinear equations. On the other hand, by putting $T_a = \beta T_c$ (in particular, $\beta = 1$), it is possible to find a relationship between the lengths that ensures these conditions. The PE for vacuum RT structures should be solved at a very high current density, when a significant change in the quantum potential used in the SE is possible due to the spatial charge. At the same time, a high current density results in the heating and the need to solve the Fourier thermal conductivity equation for thermal conductivity together with the SE and PE, also, preferably in a non-stationary form. This is a complex nonlinear problem that requires an iterative solution.

Heat generation due to the Nottingham effect at the cathode and due to the ingress of accelerated electrons to the anode occurs at their surfaces at a length of the order of the FPL, which results in heating of the electrode surfaces. The tunneling area size should be an order of magnitude smaller than the FPL in the corresponding materials, which limits the possible number of electrodes, while in the tunneling area the transport is ballistic, i.e. there is no scattering and heat dissipation. Heat generation occurs only at the cathode and anode, i.e. the thermal problem should be solved only on these electrodes. The well-known Peltier effect occurs when the current passes through the contact of two metals with different FE values. A similar effect is considered in [51] in case of tunneling through a single barrier and it is shown that under certain rather rare conditions, it is possible to cool the anode with electrons of certain energies. These conditions are determined by a low anode voltage and a significantly higher FE of the anode compared to the FE of the cathode. However, a significant reverse tunneling current is possible from the anode to the cathode and heating of the anode due to the Nottingham effect under such conditions especially in case of RT. The complete thermal balance is considered in this paper.

CNT piles can serve as good structures for grids. It is technologically convenient to use grid and anode electrodes with the same positive potential $U_g = U_a$, separated by

dielectric substrates and made in the form of a single block (Fig. 1). There may be several grid electrodes with different grid voltages. Next, the index $B$ denotes the size of the barrier, the index $W$ denotes the size of the well, and $t_w = t_g$. It is convenient to take $U_g = U_a = E_{Fc}/e$ for RT, where $E_{Fc}$ is cathode FE. In this case, all potential wells have a bottom of the same level, coinciding with the bottom of the cathode conduction band. It is desirable to align the height of the barriers for RT, which can be easily done by changing the DP $\varepsilon_n$ and the thickness of the dielectric layers $t_n$. Papers [22,49,50] consider the cases when dielectric films partially fill the cathode–anode space. The higher the fill factor, the higher the tunneling coefficient. The results of the analysis show that the case of complete filling of the gap is more interesting, since it results in a greater decrease (by $\varepsilon_n$ times) of the heights of the barriers. Heat is released on the anode due to Joule heat, as well as due to the excess kinetic energy of electrons during their scattering and transition to the anode FL. However, heat absorption (cooling of the anode) is also possible in the case of electron tunneling from low levels at the cathode below the anode FL, if this is possible. The temperatures of the cathode and anode surfaces are generally different. The radiation heat transfer should be taken into account if the cathode and anode are separated by a vacuum gap. It is negligible in case of a temperature difference of less than 1000 K. Diamond ($\varepsilon = 5.6$) or BeO ($\varepsilon = 2.955$) with high thermal conductivity can be used as a dielectric to equalize the temperatures of the cathode and anode. Diamond is more preferable because its thermal conductivity is higher and the barriers are almost twice as low. Additionally, it has greater electrical strength, since the conductivity of BeO at 700 K is $10^{-2}$ S/m. $SiO_2$ can be another possible good dielectric for manufacturing of RTS.

## 2. Determination of quantum potentials

We will limit ourselves in this study to relations of the type (13), (14), determining the set temperatures while neglecting radiative heat transfer, solving the SE with the definition of $D^{\pm}$ at defined temperatures with the calculation of integrals (4), (5). The subject structures (Fig. 1) can be either with RT, or without it, depending on the configurations of the grids and the voltages on them. $V(x) = V_0(x) + V_a(x)$ should be taken in case of a diode structure, where $V_a(x) = -xeU_a/d$, and the part of the potential associated with multiple images is given by the ratio [22]:

$$V_0(x) = E_{Fc} + \frac{W_c}{\varepsilon} - \frac{e^2}{16\pi\varepsilon_0\varepsilon}\left\{\frac{1}{x+\delta_c} + \frac{2x^2}{d(d-x+\delta_a)(d+x)} + \frac{2x^2}{d^3}\sum_{n=2}^{\infty}\frac{1}{(n^2-(x/d)^2)n}\right\}. \quad (15)$$

Here, the parameters $\delta_{c,a}$ are related to the work function (WF) from the cathode $W_c = e^2/(16\pi\varepsilon_0\delta_c)$, WF from the anode $W_a = e^2/(16\pi\varepsilon_0\delta_a)$ and are introduced based on experimental data. $V(0) = V_0(0) = E_{Fc}$ on the cathode. $V(d) = E_{Fc} + (W_c - W_a)/\varepsilon - eU_a$ on the anode. All energy levels at the anode are reduced by $eU_a$ if cathode and anode materials and WF are the same. The energy for such an energy diagram is counted from the bottom of the cathode conduction band, the barrier relative to the FE has a height of $W_c/\varepsilon$ at a large size of $d$, and the barrier decreases due to the Schottky effect at small values of $d$. Equation (15) and calculation $V(x)$ should be applied to the diode structures for which they are written, and the potential should be crosslinked in case of several electrodes. Such an arrangement is required for each of the dielectric (vacuum) gaps in the case of several electrodes, taking into account that the potentials on the electrodes are set and constant, and then it is necessary to use the continuity of the potential.

Reduction of the barrier by $\varepsilon = 5.6$ times for diamond results in an increase of the current of the tunnel diode by 3 or more orders of magnitude. A single barrier in the diode structure in work [52] is approximated by a parabola in the absence of the anode voltage. The dependence (14) is conveniently approximated more precisely by the following expressions for $W_c = W_a = W = e^2/(16\pi\varepsilon_0\delta)$ and $E_{Fc} = E_{Fa} = E_F$.

$$V_0(x) \approx E_F + W(1-\alpha/d)[1-(2x/d-1)^4]/\varepsilon, \quad (16)$$

$$V_0(x) \approx E_F + W\frac{(1-\alpha/d)(1+\delta/d)^2}{(1-\delta/d)^2\varepsilon} \times \left[1 - \frac{\delta d}{\big(z+\delta(1-x/d)\big)\big(d-z+x\delta/d\big)}\right], \quad (17)$$

$$\alpha = 2\delta + \delta\sum_{n=1}^{\infty}\frac{1}{(2n-1)n(2n+1)} = \delta\big(2\ln(2)+1\big).$$

$V_0(0) = V_0(d) = E_F$ in this case follows from the fact that

$$\sum_{n=1}^{\infty}\frac{1}{n(n+1)(n+2)} = \frac{1}{4}.$$

In all these cases, $\delta/d \sim 10^{-2}$, and the error of the specified ratios is of the order of $\delta^2/d^2 \sim 10^{-4}$. The ratio (17) is somewhat more accurate than (16). Figure 2 shows a comparison of the results of (15)–(17). There are also results for approximating a parabola and a sixth-order parabola. The parabolic approximation provides a pointed vertex, and the sixth-order parabola approximation provides a more flattened vertex. In the case of different cathode and anode materials, the value $(W_a - W_c)x/(\varepsilon d)$ should be added to (16) and (17). In the case of several electrodes, the specified ratios should be applied sequentially. An example of their application is shown in Fig. 3–6. Fig. 3 corresponds to the quantum heterostructure GaAs–AlAs. Fig. 4 corresponds to a vacuum triode with one quantum well, and Fig. 5, 6 corresponds to a vacuum diode. Figure 6 illustrates the effect on the potential of dielectric films

and carbon structures on a metal cathode. We obtain a solution of the SE using the obtained analytical dependences $V(x)$ without taking into account the spatial charge, i.e. at a relatively low current density. The contribution to the potential in case of its high density is estimated in the study [23], and the corresponding formula is given below.

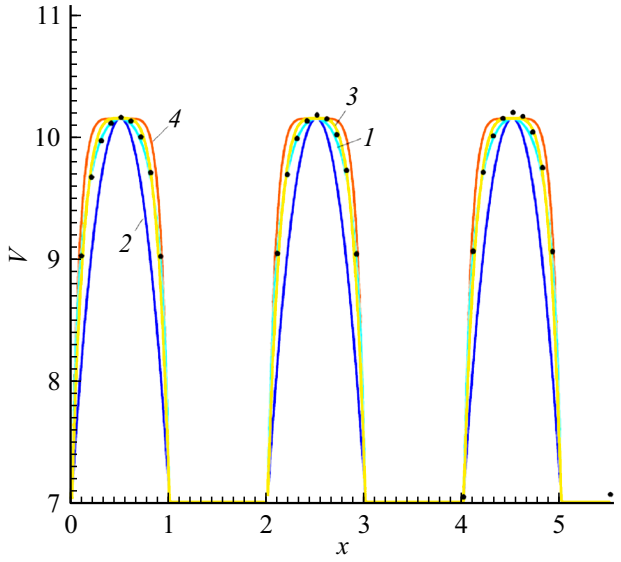


**Figure 2.** Comparison of approximation ($V$, [eV], $x$, [nm]) by formula (2) (curve *1*), parabolic approximation (curve *2*), approximations by a parabola of the fourth (*3*) and sixth orders (*4*) with exact [19] profile (symbols ***) of the quantum potential (*5*) in RTS with two wells (double grid) at the size of gaps (barriers) $t_B = 1$, the size of wells (grids) $t_W = 1$ (nm) at $E_{Fc} = 7$ eV and $U_g = U_a = 0$.

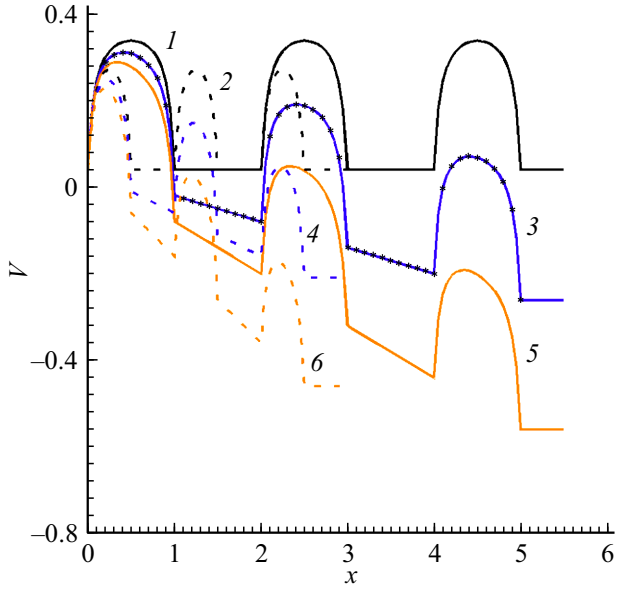


**Figure 3.** Profiles $V$, [eV] depending on the coordinate $x$, [nm] for semiconductor double-core RTDs at $t_B = t_W = 1$ nm (solid curves) and $t_B = t_W = 0.5$ nm (dashed curves) at different anode voltages (V): $U_a = 0$ (curves *1, 2*), 0.25 (*3*), 0.3 (*4*), 0.5 (*5*), 0.6 (*6*).

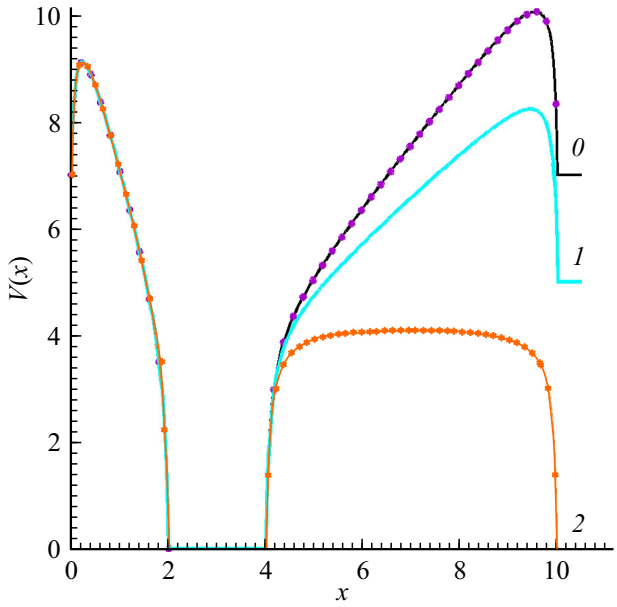


**Figure 4.** Quantum potential distribution $V$, [eV] in a vacuum triode depending on the coordinate $x$, [nm] at $d = 10$ nm, grid voltage 7 V and different anode voltages (V): 0 (curve *1*), 2 ( it2), 7 (*3*). $E_F = 7$, $W = 4.36$ eV. Grid size 2 nm.

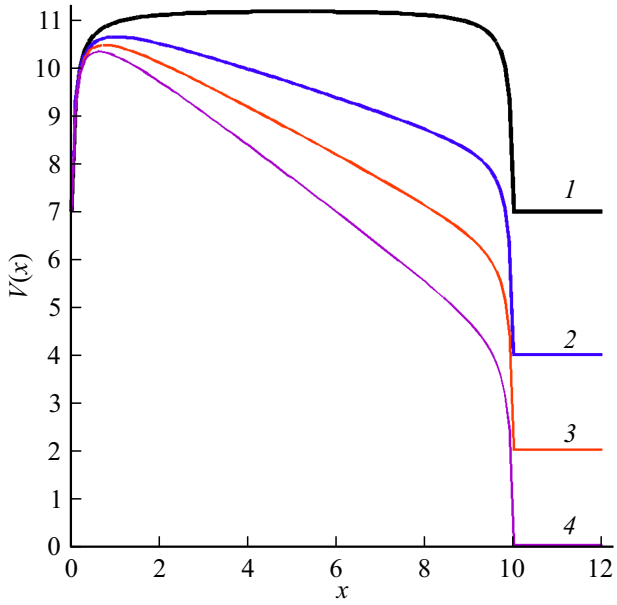


**Figure 5.** Shape of the potential barrier $V$, [eV] in a vacuum diode $d = 10$ nm depending on the coordinate $x$, [nm] at different anode voltages (V): 0 (curve *1*), 3 (*2*), 5 (*3*), 7 (*4*). $E_F = 7$, $W = 4.36$ eV.

## 3. One-dimensional SE solution and current calculation

In our case, the easiest way to obtain a solution for the SE is by using the method of wave impedance transformation, since the wave function itself (WF) as such does not interest us. We only need permeabilities $D^{\pm}$. A small section

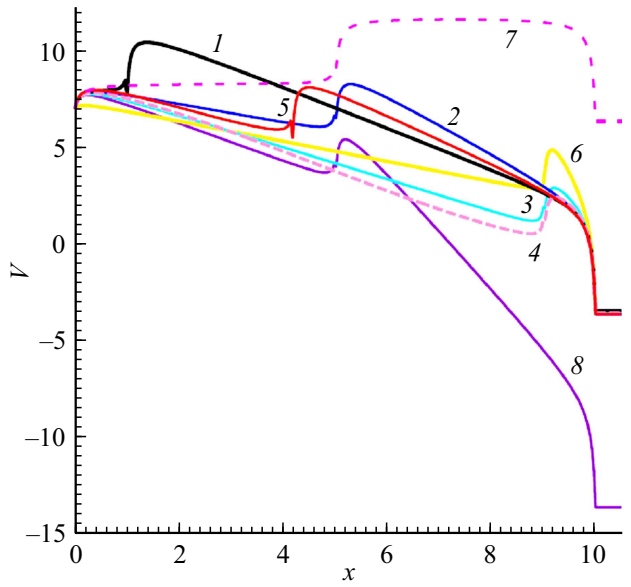


**Figure 6.** Calculations of the quantum potential $V$, [eV] in the diode depending on the coordinate $x$, [nm] in the presence of structures on the cathode: glassy carbon-CNT (curves *1–4*), CNT pile (*5*), dielectric film (*6–8*). The dimensions are $t$, [nm]: 1 (curve *1*), 5 (*2, 7, 8*), 4.18 (*5*), 9 (*3, 4, 6*). $W_c = 4.36$, $W_a = 5.5$ eV. Curves *1–6* are constructed for $U_a = 10$ V, curve *7* is constructed for $U_a = 0$, curve *8* is constructed for $U_a = 20$ V.

$|x-x_n| \le \Delta x/2$ can be described by the wave function

$$\psi(x) = \psi_n(x) = A_n^+ \exp(ik_n x) + A_n^- \exp(-ik_n x)$$

and its derivative, for which

$$\psi_n'(x) = ik_n A_n^+ \exp(ik_n x) - ik_n A_n^- \exp(-ik_n x).$$

The matching of these functions can be performed based on the transfer matrix method [22]. The use of the sweep method is another solution. We have $\psi_n'' = (\psi_{n+1} - 2\psi_n + \psi_{n-1})/\Delta x^2$ for it. By imposing boundary conditions

$$\psi_0 = A(E)\big(1 + R(E)\big),$$

$$\psi_0' = ik_c(E)A(E)\big(1 - R(E)\big) = (\psi_1 - \psi_0)/\Delta x,$$

$$\psi_N = A(E)T(E),$$

$$\psi_N' = ik_a(E)T(E)A(E) = (\psi_N - \psi_{N-1})/\Delta x,$$

we obtain

$$2k_c(E)A(E)\Delta x = -i\psi_1 + \psi_0\big(k_c(E)\Delta x + i\big),$$

$$\psi_{N-1} = \psi_N\big(1 - ik_a(E)\Delta x\big).$$

This allows calculating the wave function at all discrete points using the formula

$$\psi_{n+1} = \left(2 + \frac{2m_e\Delta x^2}{\hbar^2}(E - V_n)\right)\psi_n - \psi_{n-1}, \qquad (18)$$

if, for example, $\psi_0 = 1$ is used. The real value of $\psi_0$ can be found by comparing the calculated value of $\psi_N$ with $\psi_{N-1}/\big(1 - ik_a(E)\Delta x\big)$. It is more convenient to use a backward sweep. All values in this case are proportional to $\psi_N$, the reflection coefficient does not depend on $\psi_N$ and is calculated immediately:

$$R(E) = \frac{ik_c(E)\Delta x - \psi_1/\psi_0}{ik_c(E)\Delta x + \psi_1/\psi_0}.$$

SE can be solved using the series method. It is convenient to use the functions $\cos(n\pi x/d)$ and $\sin(n\pi x/d)$ for this purpose [23]. The series method is convenient for the joint solution of non-stationary SE, Fourier thermal conductivity equation and PE. In this case, it consists in obtaining equations for time-dependent expansion coefficients. The self-consistent solution of the above equations together with the problem of radiative heat transfer between the anode and cathode results in a complex highly nonlinear non-stationary problem. Such a problem, for example, is typical for explosive emissions.

The method of transformation of normalized wave impedances $\eta_n = k_0/k_n$, where $k_n = \sqrt{2m_e\big(E - V(x_n)\big)}/\hbar$, is more convenient. $k_c = k_0 = \sqrt{2m_e E}/\hbar$ on the cathode, $k_a = \sqrt{2m_e\big(E - V(d)\big)}/\hbar$ on the anode. By sequentially transforming the impedance of the anode to the impedance of the cathode according to the following formula

$$Z_{l-1} = \eta_l \frac{Z_l - i\eta_l \tan(k_l t_l)}{\eta_l - iZ_l \tan(k_l t_l)}, \qquad (19)$$

$$l = N, N-1, \ldots, 2, 1,$$

$$Z_N = Z_a = \eta_a = k_0/k_a,$$

we obtain the reflectance at the cathode

$$R_c(E) = (Z_0 - \eta_0)/(Z_0 + \eta_0)$$

and the permeability $D^+(E) = 1 - |R_c(E)|^2$. We obtain $D^-(E) = 1 - |R_a(E)|^2$ by transforming from the cathode to the anode. $E > 0$ should now be taken at the anode in this case, counting the energy from the bottom of the anode conduction band. At the same time, all energy levels at the cathode increase by the value of $eU_a$.

Let's consider the simplest analytical model of a tunnel diode with a rectangular barrier as an example. Let the electrode materials be the same. The height of the barrier relative to FL is taken to be equal to $W$, i.e. relative to the bottom of the cathode conduction band $V = E_F + W$, and relative to the bottom of the anode conduction band $V = E_F + W + eU_a$. Let this barrier exist in the area $0 < z < d$. $k = i\sqrt{2m_e(E_F + W - E)}/\hbar$ in the barrier in the first case and the normalized impedance is $\tilde{\eta} = -i/\sqrt{(E_F + W)/E - 1}$. It is normalized to $n_c$. We have the step $V_a = E_F - eU_a$ and the parameters $k_a = \sqrt{2m_e(E + eU_a)}/\hbar$, $\tilde{\eta}_a = 1/\sqrt{1 + eU_a/E}$ in the area

$z > d$. $k_c = k_0 = \sqrt{2m_e E}/\hbar$, $\tilde{\eta}_c = 1$ at the cathode. We obtain the input impedance, reflectance and permeability:

$$Z_0 = |\tilde{\eta}| \frac{\tilde{\eta}_a - i|\tilde{\eta}| \tanh(|k|d)}{|\tilde{\eta}| + i\tilde{\eta}_a \tanh(|k|d)},$$

$$R_c(E) = \frac{Z_0 - 1}{Z_0 + 1} = \frac{|\tilde{\eta}|\tilde{\eta}_a - |\tilde{\eta}| - i(|\tilde{\eta}|^2 + \tilde{\eta}_a)\tanh(|k|d)}{|\tilde{\eta}|\tilde{\eta}_a + |\tilde{\eta}| - i(|\tilde{\eta}|^2 - \tilde{\eta}_a)\tanh(|k|d)},$$

$$|R_c(E)|^2 = \frac{|\tilde{\eta}|^2(\tilde{\eta}_a - 1)^2 + (|\tilde{\eta}|^2 + \tilde{\eta}_a)^2 \tanh^2(|k|d)}{|\tilde{\eta}|^2(\tilde{\eta}_a + 1)^2 + (|\tilde{\eta}|^2 - \tilde{\eta}_a)^2 \tanh^2(|k|d)},$$

$$D^+(E) = \frac{4|\tilde{\eta}|^2\tilde{\eta}_a\left(1 - \tanh^2(|k|d)\right)}{|\tilde{\eta}|^2(\tilde{\eta}_a + 1)^2 + (|\tilde{\eta}|^2 - \tilde{\eta}_a)^2 \tanh^2(|k|d)} \leq 1.$$

In the case of a broad barrier

$$\tanh^2(|k|d) = 1 - 4\exp(-2|k|d),$$

and we have

$$D^+(E) \approx \frac{16|\tilde{\eta}|^2\tilde{\eta}_a \exp(-2|k|d)}{(|\tilde{\eta}|^2 + 1)\tilde{\eta}_a^2 + |\tilde{\eta}|^2 + |\tilde{\eta}|^4}.$$

In the case of a broad and high barrier $|\tilde{\eta}| \ll 1$, and then

$$D^+(E) \approx \frac{16|\tilde{\eta}|^2\tilde{\eta}_a \exp(-2|k|d)}{\tilde{\eta}_a^2 + |\tilde{\eta}|^2}.$$

In case of high voltage at the anode $\tilde{\eta}_a \ll 1$. In all these cases $D^+(E) \ll 1$. In the case of an extremely narrow ($d \to 0$) barrier $D^+(E) = 4\tilde{\eta}_a/(\tilde{\eta}_a + 1)^2 \leq 1$. The equality is achieved at $\tilde{\eta}_a = 1$ or at $U_a = 0$. Non-zero voltage always results in the reflection. Tunneling from the anode is not possible if $E < 0$, since there are no negative levels at the cathode. Electrons leave the anode to the source with FE $E_{Fa}$. We obtain the following by transforming the wave impedance of the cathode $\tilde{\eta}_c = \sqrt{E/E_F}$ to anode

$$Z_a = |\tilde{\eta}| \frac{\tilde{\eta}_c - i|\tilde{\eta}| \tanh(|k|d)}{|\tilde{\eta}| + i\tilde{\eta}_c \tanh(|k|d)},$$

$$R_a(E) = \frac{|\tilde{\eta}|(1 - \tilde{\eta}_c) + i(\tilde{\eta}_c + |\tilde{\eta}|^2)\tanh(|k|d)}{|\tilde{\eta}|(1 + \tilde{\eta}_c) + i(\tilde{\eta}_c - |\tilde{\eta}|^2)\tanh(|k|d)},$$

$$|R_a(E)|^2 = \frac{|\tilde{\eta}|^2(1 - \tilde{\eta}_c)^2 + (\tilde{\eta}_c + |\tilde{\eta}|^2)^2 \tanh^2(|k|d)}{|\tilde{\eta}|^2(1 + \tilde{\eta}_c)^2 + (\tilde{\eta}_c - |\tilde{\eta}|^2)^2 \tanh^2(|k|d)},$$

$$D^-(E) = \frac{4|\tilde{\eta}|^2\tilde{\eta}_c\left(1 - \tanh^2(|k|d)\right)}{|\tilde{\eta}|^2(1 + \tilde{\eta}_c)^2 + (\tilde{\eta}_c - |\tilde{\eta}|^2)^2 \tanh^2(|k|d)} \leq 1.$$

Permeability is low at $\tilde{\eta}_c \gg 1$ (i.e. at $E \gg E_F$): $D^-(E) \approx 4\sqrt{E_F/E}$. The value of $\tilde{\eta}_c$ is small at $E \ll E_F$, and the permeability of $D^-(E) \approx 2\tilde{\eta}_c \exp(-2|k|d)/(1 + |\tilde{\eta}|^2)$ is exponentially low. In reality, the model in the form of a rectangular barrier is very inaccurate. It can be used for wide barriers and small values $eU_a$ compared to WF and FE. In reality, the barrier is close to a triangular shape, placed on a rectangular pedestal. Such a barrier reflects significantly less than a rectangular barrier of the same width. Modeling of RTS with several rectangular barriers requires correction of their widths [23]. The width and height of a single barrier decreases with an increase of the anode voltage $U_a$. It disappears at a critical field $E_{xc} = U_a/d = 16\pi\varepsilon_0 W^2/e^3$ , forming a bevel to the anode, while the transparency of the FL cathode may be close to unity. $E_{xc} = 5.7 \cdot 10^{10}$ V/m at $W = 4.5$ eV. Voltages one order of magnitude lower already provide permeability several orders of magnitude less. RT makes it possible to obtain permeability of $D = 1$ for some energies, while it is important that they can be significantly lower than the FL cathode. This theoretically makes it possible to increase the tunneling current by several orders of magnitude at fields significantly lower than the critical level. Usually, the shapes of single and multiple barriers are considered rectangular for simplicity. Quantum approaches to determining the WF and the shape of barriers are very complex and difficult to implement in the problems of calculating the emission current. The WF can be calculated using the density functional theory method, but its experimental values can be used more accurately. Formally, the quantum potential for SE should be calculated, depending on the spatial charge density of the ejected electrons in the vacuum region and with several electrodes, which is difficult to perform using the quantum approach. In reality, the profile of simple and complex barrier structures — quantum potential $V(z)$ — can be strictly determined by the method of multiple images [22,49,50] Fig. 3–6. It is close to a triangle placed on a rectangular pedestal between two electrodes with high voltage (e.g. in diode) (Fig. 5). It is close to an inverted parabola of the fourth degree placed on a pedestal between two close electrodes with the same potential (for example, two grids) (Fig. 2, 3, 5). It should be noted that there are levels at the cathode at $T = 0$ that are higher than the levels at the anode. For them always $D^+ \gg D^-$ at $eU_a > 1$ eV and they determine the main current. Therefore, the current from the cathode is always greater than the current from the anode, although the thermal current from a highly heated anode may be greater than the thermal current from a colder cathode. The heating of the anode increases with an increase of $U_a$. Increase of $U_a$ reduces $W$. The greater is the $d$ and the voltage the closer the shape is to triangular. Calculations show that a triangular barrier is more permeable than a rectangular one of the same height and width, and it is necessary to reduce the width of the rectangular barrier by more than two times for obtaining the same permeability. Therefore, the above analytical relations can be used for low voltages and for sufficiently high temperatures when a single barrier is still close to a rectangular one, i.e. in the case of thermal emission. There are electrons of all energies at a non-zero temperature, and the parameters $k = \sqrt{2m_e(E - E_F - W)}/\hbar$ and $\eta = 1/\sqrt{1 - (E_F + W)/E}$ become valid when the energies of the barrier height are exceeded, while

$$Z_0 = \eta \frac{\eta_a - i\eta \tan(kd)}{\eta - i\eta_a \tan(kd)},$$

$$|R_c(E)|^2 = \frac{\eta^2(\eta_a-1)^2 + (\eta^2-\eta_a)^2\tan^2(kd)}{\eta^2(\eta_a+1)^2 + (\eta^2+\eta_a)^2\tan^2(kd)},$$

$$D^+(E) = \frac{4\eta^2\eta_a}{\eta^2(\eta_a+1)^2 + [(\eta^2+\eta_a)^2 - \eta^2(\eta_a+1)^2]\sin^2(kd)}.$$

High energies $E \gg eU_a$ and $E \gg E_F$ will result in $\eta_a = 1 - eU_a/(2E)$, $\eta = 1 - (E_F+W)/(2E)$. We obtain $D^+ = 4\eta_a/(\eta_a+1)^2 \le 1$ and $D^+ \approx 1 - e^2U_a^2/(4E^2)$ at $kd = n\pi$. $D^+ = 4\eta^2\eta_a/(\eta^2+\eta_a)^2 \le$ at $kd = (2n-1)\pi/2$, and $D^+ \approx 1 - (E_F+W)^2/E^2 - e^2U_a^2/(4E^2)$ at high energies. Usually $W \ll E_F$ with $eU_a = E_F$, and then $D^+ \approx 1 - 5e^2U_a^2/(4E^2)$. It is possible to use average value of $D^+ \approx 1 - 3e^2U_a^2/(4E^2)$. Usually it is assumed that $D^+ = 1$ in case of thermal emission, or a small correction for the unit deviation of permeability is determined and an adjusted Richardson formula is obtained. The following approximation can be used in case of $E \gg eU_a$

$$D^+(E) \approx 1 - \frac{(E_F + W + eU_a/2)}{E}\sin^2(kd). \qquad (20)$$

It is necessary to calculate permeability $D^\pm$ for each energy and in broad energy ranges for a rigorous analysis of TFE, and it is necessary to numerically determine integrals (4), (5) with them. Numerical estimates show that it is sufficient to take the upper limit $3E_F$ for $T < 2500$ K. It is difficult to obtain accurate analytical expressions mainly due to the complexity of defining $D^\pm$. If tunneling from the anode is impossible in the RTS at $eU_a > E_{Fc}$ and $T = 0$, then there are always energies at the final temperature that coincide with the resonant levels for which $D^- = 1$. In the general case, this requires taking into account both formulas (4), (5) and solving the SE for the corresponding quantum potentials.

Let's consider the simplest case $T_c = T_a = T$, which can be achieved by selecting electrode lengths and conditions for RTS with a single grid. The condition $U_g = U_a$ means that the bottom of the well coincides with the maximum energy at the anode at $T = 0$. The bottom of the well and the maximum energy at the anode corresponds to zero if $U_g = U_a = E_F/e$. In this case, RT is possible only from the cathode. In this case, the integral (1) can be replaced by the sum

$$J(U_a) = J^+(U_a) \approx \frac{-em_e}{2\pi^2\hbar^3}\sum_{n=1}^{N}(E_{Fc} - E_n')E_n'' \qquad (21)$$

of the resonant energy levels $E_n = E_n' - iE_n''$. The specified complex resonance levels should be found from the condition $R_c(E_n)$. We obtain $D^+(E_n) = D^-(E_n)$ for $T > 0$ , but $dn_E^+ \gg dn_E^-$, and $J^-$ can be neglected according to (3). We obtain $D^+(E_n) \approx D^-(E_n) \approx 1$ in the region $E \gg E_{Fc}$ and the following ratios for densities

$$dn_E^+ = \frac{m_e k_B T}{2\pi^2\hbar^3}\exp\left(-\frac{E-E_F}{k_B T}\right)dE,$$

$$dn_E^- = \frac{m_e k_B T}{2\pi^2\hbar^3}\exp\left(-\frac{E+eU_a-E_F}{k_B T}\right)dE = \exp\left(-\frac{eU_a}{k_B T}\right)dn_E^+,$$

that also satisfy the condition $dn_E^+ \gg dn_E^-$ at a not too high temperature. Integrals (4) and (5) are divided into the regions $0 < E < E_F$ and $E_F < \nu E < \infty$, where $\nu \sim 3$–$4$. $k_B T = 0.026$ eV at room temperature. We have $k_B T = 0.217$ eV at the maximum operating temperature of $T = 2500$ K, therefore, the following estimate can be obtained taking the upper limit $E_F$

$$-J^-(U_a, T) = \frac{em_e k_B T}{2\pi^2\hbar^3}\int_0^{E_F} D^-(E, U_a)\exp\left(-\frac{E}{k_B T}\right)dE$$

$$< \frac{em_e(k_B T)^2}{2\pi^2\hbar^3}\left(1 - \exp\left(-\frac{E_F}{k_B T}\right)\right).$$

Here we majored the integral and took the electrodes the same. The incoming exponent is $10^{-14}$ even for the highest temperatures, and the integral itself is less than $0.001$ A/m$^2$ for all temperatures. The calculation at $T = 0$ gives the maximum values of $j^+ \sim 10^{12}$–$10^{13}$ A/m$^2$ in case of RT. The majority estimate was obtained at $D^- = 1$. In reality, this value can be achieved at some points of $E_n'$ at $E_n''/E_n' \sim 10^{-3}$ in case of resonant tunneling, between which the permeability is several orders of magnitude lower. We obtain an estimate of $|j^-| \sim 10^{-6}$ A/m$^2$ taking the average value of $\bar{D}^- = 0.001$. Therefore, the backward current can be completely neglected in case of resonant tunneling. This is also true in a conventional non-resonant (diode) structure. A small compared to $k_B T$ or a comparable value of $eU_a$ can be considered to be the only condition for a significant backward current. In this case, the backward current can be greatly increased in comparison with the direct current by exceeding the temperature of the anode in comparison with the cathode. The remainder of the integral can be estimated by analytical calculation

$$\int_{\nu E_F}^{\infty}\left(1 - \frac{3e^2U_a^2}{4E^2}\right)\exp\left(-\frac{E-E_F}{k_B T}\right)dE \approx k_B T$$

$$\times \exp\left(-\frac{(\nu-1)E_F}{k_B T}\right)\left(1 - \frac{3e^2U_a^2}{4(\nu E_F)^2}\right).$$

It can be seen from this the specified remainder is so small that it may be neglected in case of $\nu = 3$, when these ratios are fulfilled with good accuracy. Therefore, it is possible to limit the integral to the upper limit $3E_F$. In reality, this limit can even be lowered.

Fig. 4 shows the distribution of potential in a structure with a single grid (one well) at different voltages on the grid. The structure is chosen to be asymmetric without RT. Permeabilities $D^+$ are plotted for this structure in Fig. 7 and dependences of current density on temperature at different anode voltages are plotted in Fig. 8. Fig. 9 shows permeabilities for RTS with one and two wells. A thin layer of barium on copper was considered. The RT is not complete in the structure shown in Fig. 7, whereas Fig. 9 shows several RT peaks. A cathode with a low WF (barium)

and grid electrodes with an increased WF (platinum) were taken to align the barriers. The use of RTS with one and two grid electrodes is very promising as vacuum sources of electrons in the designs of electronic devices, in particular, electronic guns for the TWB of a THz range. There is a current from the cathode to the anode in all such structures, but there is also a backward tunneling current from the anode to the cathode. It is usually extremely small. It

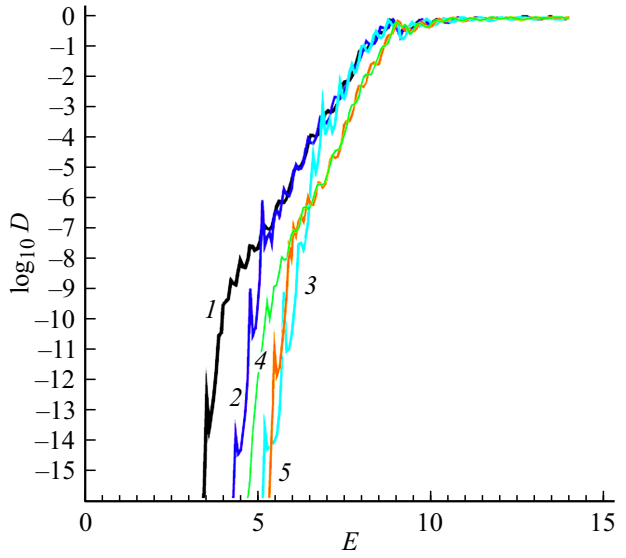


**Figure 7.** Permeability depending on the kinetic energy of electrons $E$, [eV] in a triode nanostructure at different voltages (V) on the grid and anode: $U_g = 7$, $U_a = 7$ (curve *1*); $U_g = 7$, $U_a = 5$ (*2*); $U_g = 7$, $U_a = 3$ (*3*); $U_g = 5$, $U_a = 7$ (*4*); $U_g = 5$, $U_a = 5$ (*5*).

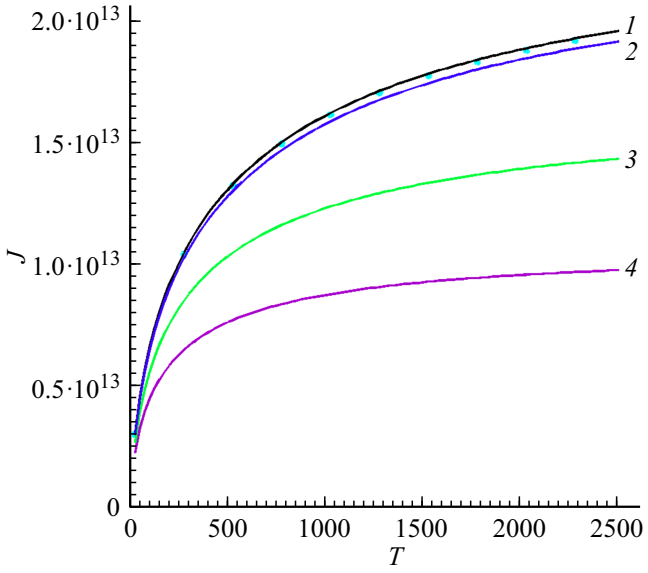


**Figure 8.** Temperature dependence of current density $J$, [A/m$^2$] in a triode nanostructure at different voltages (V) on the grid and anode: $U_g = 7, U_a = 7$ (curve *1*); $U_g = 7, U_a = 3$ (*2*); $U_g = 5$, $U_a = 7$ (*3*); $U_g = 3$, $U_a = 7$ (*4*). The asterisks *** indicate the results for $U_g = 7$, $U_a = 5$. $E_F = 7$ eV, $W = 4.36$ eV.

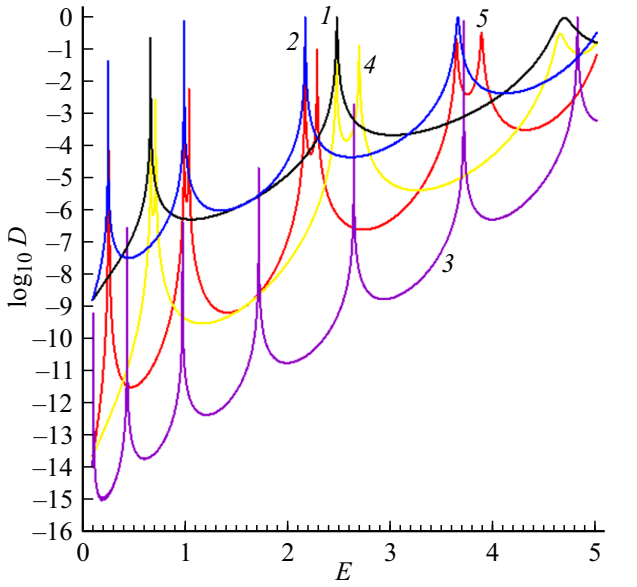


**Figure 9.** Permeability $D$ depending on the energy of (eV) single-well (curves *1–3*) and double-well (*4, 5*) RTS for barriers $t_B = 0.6$ nm (*1, 2, 4, 5*) and $t_B = 1$ nm (*3*). Curves *1, 4* are plotted for wells with $t_W = 0.6$ nm, curves *2, 5* for $t_W = 1.2$ nm, curve *3* for $t_W = 2$ nm. The values $W_c = 2.5$, $E_{Fc} = 5$, $W_g = 6.35$ eV were used.

should be taken into account at low or alternating voltages at the anode. The backward current is exponentially small in our case of significant anode voltage. It is necessary to modify the potential used above for taking into account the spatial charge. The modification has the following form if the gap is completely filled with a dielectric

$$V_a(x) = -\frac{eU_a x}{d} - \frac{2ed}{\pi^2 \varepsilon \varepsilon_0} \sum_{n=1}^{\infty} \int_0^d |\psi(x')|^2 n^{-2} \sin\left(\frac{n\pi x}{d}\right) \times \sin\left(\frac{n\pi x'}{d}\right) dx'. \tag{22}$$

Partial or inhomogeneous filling requires a numerical solution of PE. The solution (22) is applicable to several electrodes. It is necessary to use an iterative procedure for calculating the wave function and current density based on the consideration of the spatial charge. If the grid voltage is greater than the anode voltage, then the last barrier at the anode has a bevel towards the cathode (Fig. 4). The counting from the bottom of the cathode conduction band and at $U_a = U_g = EF_c$ will provide $V_a = V_g = 0$. We consider the grids to be an order of magnitude thinner than FPL. Then the electron transport is ballistic without scattering. The constant quantum potential corresponds to FL with this definition, $V(z)$ on the grids and on the anode.

The following is apparent without taking into account the spatial charge if there is a non-conductive ideal dielectric

film with a thickness of $t$ on the cathode, and there is a vacuum in the region of $t < z < d$

$$V_a(x) = -eU(x) = -eU_a \times \begin{cases} x/[\varepsilon d + (1-\varepsilon)t], & 0 \le x \le t, \\ \big(\varepsilon x + t(1-\varepsilon)\big)/[\varepsilon d + (1-\varepsilon)t], & t < x \le d. \end{cases}$$

This function satisfies the Laplace equation and the boundary conditions at the cathode $V_a(0) = 0$, at the anode $V_a(d) = -eU_a$ and at the dielectric boundary (it is continuous and creates continuous induction). The values of the function $V_0(x, t, \varepsilon)$ are also used in [22,49,50] when the region is partially filled with a dielectric, instead of the function (15). Such a function requires the construction of multiple images relative to two metallic and one dielectric surface, i.e. has a significantly more complex appearance. The method is based on the introduction of the coefficient of reflection of the electrostatic induction flux $(1-\varepsilon)/(1+\varepsilon)$ from the surface of the dielectric. The coefficient of reflection from the metal corresponds to an infinite DP and is equal to $-1$. The dielectric layer on the cathode greatly increases the number of images. The function constructed in this way has the properties $V_0(x, d, \varepsilon) = V_0(x)$, $V_0(x, t, 1) - E_{Fc} = \varepsilon\big(V_0(x) - E_{Fc}\big)$. It also takes into account the WF from the dielectric. Figure 6 shows the results of constructing a quantum potential for structures with partial dielectric filling. It should be noted that semiconductor and carbon structures can have both free and bound charges at the cathode (for example, $\pi$-electrons). The film can have both dielectric and metallic properties depending on the concentration of $N_e$ and the ratio of thickness $t$ and the length of the Debye shielding $L_D = \sqrt{\varepsilon_0 \varepsilon k_B T/(N_e e^2)}$. The field penetrates into a part of the film in the intermediate case. The penetration of the field into the film results in a bevel of the potential to the barrier (Fig. 6). This bevel results in the acceleration of electrons running into the barrier. The barrier arises mainly beyond the boundary of the dielectric and the vacuum. The film occupying a significant part of the gap results in the dimensional effect of narrowing the barrier [22,49,50]. The curves *3, 4* in Fig. 6 are constructed taking into account the solution of the PE for the concentration of electrons in the film.

Let's consider the diode RTS from $Ga_{1-x}Al_xAs$. GaAs consists of well-conducting layers (cathode, anode and GaAs layers, which can be strongly alloyed) separated by low-conductivity layers of $Ga_{1-x}Al_xAs$, i.e. almost dielectric. The band gap of GaAs is 1.42 eV, the band gap of and AlAs is 2.16 eV at $x = 0$. The mobility of electrons $\sim 1200\,\mathrm{cm}^2 \cdot \mathrm{V}^{-1} \cdot \mathrm{s}^{-1}$ and their effective mass $\sim 0.7m_e$ at AlAs. The refraction index in the IR range is 3, i.e. DP can be considered equal to 9. We have electrons with effective mass of $0.067m_e$, mobility $8500\,\mathrm{cm}^2/(\mathrm{V} \cdot \mathrm{s})$, light holes with effective mass of $0.082m_e$ and heavy holes with effective mass of $0.45m_e$ for GaAs. Hole mobility — $400\,\mathrm{cm}^2/(\mathrm{V} \cdot \mathrm{s})$. Hole current can be neglected in the first approximation. Taking the thickness 2 nm for the AlAs layer, we obtain the barrier height of 0.45 eV considering the work function of 4.7 eV and DP 9. A height of the order of 0.38 eV is obtained with a thickness of 1 nm. Electrode alloying and performing non-alloyed GaAs regions in wells can result in a slight rise of their bottom relative to the bottom of the cathode conduction band. The application of voltage to the anode results in the addition of an appropriate potential to the reduced distribution. The additional potential in the layers can be considered as a piecewise linear function because DP weakens the electric field. The lower the potential drop, the larger the DP layer. It is easier to use the linear potential $\Phi_0(z) = -zU_a/d$ without kinks since the GaAs DP $\varepsilon = 10.9$ differs only slightly from the AlAs DP. Its superposition results in a bevel of the quantum potential profile (Fig. 3). In this case, the bottom of the wells also has a slope, which distinguishes such a structure from a structure with grids, i.e. with set potentials on conductive layers. We will denote the sizes of the areas $t_n$, $n = 1, 2, \ldots$ starting from the cathode (Fig. 1). In triode structures with the same positive grid potentials, the bottom of the pits is horizontal. It is technologically difficult to make hanging grids, so it is advisable to apply them to dielectric layers. The height of the vacuum barrier at its width $t = 2$ nm will be slightly less than WF and approximately equal to $0.86W/\varepsilon$ if the cathode WF is $W$ which for the value $W = 4.7$ eV and $\varepsilon = 10$ are approximately equal to 0.4 eV. The semiconductor RT heterostructure is usually significantly shorter than the vacuum heterostructure. A good material for grids is $n$-layered graphene. A heterostructure can be considered quantum if its length is significantly less than the FPL, otherwise it should be considered as a classical superlattice. For the latter, a series of tunneling problems should be solved, considering each electrode as macroscopic, i.e., taking into account the electron energy levels on it. Taking the FPL in GaAs 120 nm, we obtain the lengths of structures of the order of 10 nm. In graphene, it is more than an order of magnitude larger. However, this value is obtained in case of movement in the graphene plane. The movement has a perpendicular direction in a grid of $n$-layered graphene. The FPL in this direction is also large because the layers are bound by van der Waals forces at distances of 0.335 nm. This length is in the order of 50 nm in metals, i.e. it is problematic to make metal grids, since it is necessary to obtain sizes less than 2 nm. Let's assume that with a structure length of less than 20 nm, it can still be considered as a quantum one. As is known, a quantum particle penetrates the barrier without loss of energy, i.e. with the same momentum as it runs into it. This corresponds to the last turning point in a potential profile with several wells and humps. The particle moves quasi-classically after this turning point, it is accelerated by the anode, and the particle releases energy $eU_a$ when it hits the anode. The energy $E - V_{Fa}$ is released at the anode if the level $E$ from which the electron tunnels is higher than the anode FL. This energy is $E_{Fc} - E_{Fa} = eU_a$ in case of tunneling from the cathode

FL. This value can be negative in case of tunneling from deep levels and at a low potential of the anode, while the anode cools down, since the tunneled electron passes to FL [51]. The wave function at the anode can be taken as $\psi_a = T\sqrt{n(k_c)}\exp\big(ik_a(z-d)\big)$ for the diode structure, therefore $|T|^2 = k_c/k_a < 1$. Equality takes place at $U_a = 0$ when $|T|^2 = 1 - |R|^2 = D$. The quantum potential $V(x)$ is a bevel of length $d$ in case of a critical electric field at the cathode $E_{cz} = 16\pi\varepsilon_0 W^2/e^3$, which is steeper the higher the voltage. It can be approximately replaced with a step at high voltage. We obtain $1 + R = T$, $1 - R = (k_a/k_c)T$ for it, i.e. $R = (k_c - k_a)/(k_c + k_a)$. We obtain $k_a \gg k_c$ and $R \approx -1$ with a large $U_a$. A quantum particle cannot „slide“ down into an infinitely wide and deep quantum well. This explains the fact that it makes no sense to increase voltages and fields above $E_{cz}$ for increasing the current. Moreover, such fields cause local instabilities because of the atomic surface irregularities and explosive emission that destroys the cathode. RT occurs at significantly lower fields and significantly higher current densities.

Fig. 3 shows the results of calculating the quantum potential profiles of AlAs/GaAs/AlAs/GaAs/AlAs semiconductor RTS with one and two wells at different voltages at the anode based on the ratio (8). The DP everywhere is $\varepsilon = 12.9$, GaAs WF is taken equal to 4.7 eV, FE is taken equal to 0.04 eV, which corresponds to the concentration of donors in the electrodes $N = 3.6 \cdot 10^{25}\,\mathrm{m}^{-3}$. The length of the Debye shielding is $L_D = 0.7$ nm at such a concentration for room temperature, i.e. less than the length of the layer, and it can be considered almost metallic. The concentration should be increased by an order of magnitude for interpreting the layer as metallic, while the FE will increase by 4.6 times. The complex resonant frequencies obtained from the condition fully correspond to the RT peaks shown in Fig. 8, while the tunnel current density $3 \cdot 10^{13}\,\mathrm{A/m}^2$ corresponds to the structure. Such densities can be obtained for for RTS with copper electrodes and diamond films between them of size 2–3 nm.

The results of calculation of the temperature according to formulas (13), (16) depending on the length of the electrodes for the structures $1, 2, 5$ RTS are listed in the table (fig. 9). The same lengths $l_c = l_a = l$ are taken, while $J \sim 5 \cdot 10^{11}\,\mathrm{A/m}^2$. $U_a = 3.5$ V is taken for reduction of the temperature of the anode. For semiconductor RTS, the achievable current density can be at 2–3 orders of magnitude lower mainly due to the significant ohmic resistance. For GaAs $\mu = 0.067m_e$, the intrinsic semiconductor at room temperature has an electron concentration of $N = 1.8 \cdot 10^{12}\,\mathrm{m}^{-3}$. In case of doping and reaching a concentration of $N = 3.4 \cdot 10^{21}\,\mathrm{m}^{-3}$ FE at the cathode $E_{Fc} = 0.3$ eV, and a barrier height of 0.4 eV is possible. The heat dissipation can also be estimated under such conditions. RT with high current density results in heating. The cathode and anode sizes should be small, and the thermostats should be massive for reducing the operating temperatures at RT. It is convenient to use equal grid and anode voltages under the condition $U_a = E_{Fc}/e$. In this case, the barriers can be aligned by changing their sizes and changing the WF at the cathode and on the grids. It is necessary to increase the WF of the grid material in comparison with the WF of the cathode. Multilayer graphene, tungsten, palladium, platinum are such convenient materials with increased WF (respectively WF: 4.8; 4.54; 4.91–5.01; 5.0; 5.35–6.35 eV). It is possible to increase WF by fluoridation. The FE should be high at a low effective WF for the formation of deep resonant levels at the cathode. The electrode WF can be increased and barriers can be aligned by changing the electronic affinity. For example, platinum hexafluoride ($7.0 \pm 0.35$ eV) and $Pt_3Zr$ have a very high value of electron affinity. An increase of the size of the grid electrodes results in an increase of the size of the wells and an increase of the number of resonances. Barriers of several nanometers results in a decrease of the current density by orders of magnitude. They are easier to implement technologically. Usually metal films on dielectric substrates have a thickness of 2 nm and more. The thinnest single grid can be made of $n$-layered graphene. A thickness of 0.34 nm is obtained at $n = 2$ , a thickness of 1.02 nm is obtained at $n = 4$. Low voltages and shallow wells can result in a lack of resonances or in a single resonance. Thermal emission may be significant in this case.

## Conclusion

The study considers 1$D$-model of TFE in nanoscale quantum RTS with three electrodes, as well as in a diode structure, when the electrodes are heated due to the structure current. The study found conditions when backward current can be neglected in high-current structures. It should be taken into account at very low anode voltages, or with a highly heated anode. General expressions are obtained at different electrode temperatures and the heat balance is considered. The approach can be used for non-stationary processes, for which it is necessary to jointly solve the corresponding SE, PE and Fourier thermal conductivity equation. The short time of flight in such structures makes them promising for the creation of THz-band devices. The simplifications used in the analysis of heat transfer result in the need to consider the numerical results obtained as estimates. Nevertheless, the principle achievability of electrode temperatures below 2000 K at very high current densities in RTS in quasi-stationary mode was shown.

### Acknowledgments

This study was supported by grant No. 21-19-00226 from the Russian Science Foundation.

### Conflict of interest

The author declares that he has no conflict of interest.

## References


[1] D.I. Proskurovsky. *Emissionnaya elektronika* (Izd-vo TGU, Tomsk, 2010) (in Russian)

[2] C. Herring, M.H. Nichols. Rev. Mod. Phys., **21** (2), 185 (1949).

[3] W.B. Nottingham. *Thermionic Emission.* In: Electron-Emission Gas Discharges I / Elektronen-Emission Gasentladungen I. Encyclopedia of Physics / Handbuch der Physik (Springer, Berlin, Heidelberg, 1956), v. 4/21. DOI: 10.1007/978-3-642-45844-6_1

[4] G.N. Fursey. *Field Emission in Vacuum Micro-Electronics* (Kluwer Academic Plenum Publishers, Springer, NY., 2005)

[5] N. Egorov, E. Sheshin. *Field Emission Electronics* (Springer Series in Advanced Microelectronics, Springer Nature, 2017), v. 60.

[6] L. Kevin, R.G. Forbes. Surf. Interface Anal., **36**, 395 (2004). DOI: 10.1002/sia.1900

[7] R.G. Forbes. Royal Society Open Science, **6** (12), 190912 (2019). DOI: 10.1098/rsos.190912

[8] K.L. Jensen. J. Vacuum Sci. Technol. B, **21**, 1528 (2003). DOI: 10.1116/1.1573664

[9] W.W. Dolan, W.P. Dyke. Phys. Rev., **95** (2), 327 (1954). DOI: 10.1103/PHYSREV.95.327

[10] A. Modinos. *Field, Thermionic, and Secondary Electron Emission Spectroscopy* (Plenum, NY., 1984)

[11] E.L. Murphy, R.H. Good. Phys. Rev., **102** (6), 1464 (1956). DOI: 10.1103/PhysRev.102.1464

[12] S. Christov. Phys. Stat. Sol., **17** (11), 11 (1966). DOI: 10.1002/PSSB.19660170103

[13] K.L. Jensen, M. Cahay. Appl. Phys. Lett., **88** (15), 154105 (2006). DOI: 10.1063/1.2193776

[14] K.L. Jensen. J. Appl. Phys., **102**, 024911 (2007). DOI: 10.1063/1.2752122

[15] V. Semet, Ch. Adessi, T. Capron, R. Mouton, Vu Thien Binh. Phys. Rev. B, **75**, 045430 (2007). DOI: 10.1103/PhysRevB.75.045430

[16] K.L. Jensen. *A Thermal-Field-Photoemission, Model and Its Application.* In: Modern Developments in Vacuum Electron Sources, TAP, **135**, 345 (2020). DOI: 10.1007/978-3-030-47291-7_8

[17] R.G. Forbes. *Renewing the Mainstream Theory of Field and Thermal Electron Emission.* In: Modern Developments in Vacuum Electron Sources, Springer Nature, ch. 9, 2020. DOI: 10.1007/978-3-030-47291-7_9

[18] A.B. Petrin. J. Exp. Theor. Phys., **109** (2), 314 (2009). DOI: 10.1134/S1063776109080184

[19] A.B. Petrin. J. Exp. Theor. Phys., **124** (6), 854 (2017). DOI: 10.1134/S1063776117050156

[20] K.L. Jensen, M.S. McDonald, M.K. Dhillon, D. Finkenstadt, A. Shabaev, M. Osofsky. J. Vacuum Sci. Technol. B, **40**, 022801 (2022). DOI: 10.1116/6.0001656

[21] S.P. Bugaev, E.A. Litvinov, G.A. Mesyats, D.I. Proskurovskii. Sov. Phys. Usp., **18**, 51 (1975). DOI: 10.1070/PU1975v018n01ABEH004693

[22] M.V. Davidovich, I.S. Nefedov, O.E. Glukhova, M.M. Slepchenkov. J. Appl. Phys., **130**, 204301 (2021). DOI: 10.1063/5.0067763

[23] M.V. Davidovich. Tech. Phys., **67** (9), 1196 (2022)]. DOI: 10.21883/TP.2022.09.54684.257-21

[24] J. Robertson. Mater. Sci. Eng. R, **37**, 129 (2002). DOI: 10.1016/S0927-796X(02)00005-0

[25] V.I. Khvesyuk, A.S. Scriabin. High Temperature, **55** (3), 428 (2017). DOI: 10.1134/S0018151X17030129

[26] A.S. Dmitriev, *Vvedenie v nanoteplofiziku* (BINOM. Laboratoriya znanij, M., 2015) (in Russian).

[27] Y. Dubi, M. Di Ventra. Rev. Mod. Phys., **83** (1), 131 (2011). DOI: 10.1103/RevModPhys.83.131

[28] G. Chen, A. Shakouri. Trans. ASME, **124** (4), 242 (2002). DOI: 10.1115/1.1448331

[29] Y. Ezzahri, K. Joulain, J. Ordonez-Miranda. J. Appl. Phys., **128**, 105104 (2020). DOI: 10.1063/5.0017188

[30] D.G. Cahilla, W.K. Ford, K.E. Goodson, G.D. Mahan, A. Majumdar, H.J. Maris, R. Merlin, S.R. Phillpot. J. Appl. Phys., **93**, 793 (2003). DOI: 10.1063/1.1524305

[31] Y.K. Koh, D.G. Cahill, B. Sun. Phys. Rev. B, **90**, 205412 (2014). DOI: 10.1103/PhysRevB.90.205412

[32] B. Vermeersch, A. Shakouri. *Nonlocality in Microscale Heat Conduction.* https://arxiv.org/abs/1412.6555 (2014)

[33] Yu.A. Kruglyak. *Nanoelektronika „bottom-up"* (Strelbitsky Publishing House, Kiev, 2016) (in Russian).

[34] R. Tsu, L. Esaki. Appl. Phys. Lett., **22** (11), 562 (1973). DOI: 10.1063/1.1654509 (1973)

[35] L.L. Chang, L. Esaki, R. Tsu. Appl. Phys. Lett., **24**, 593 (1974). DOI: 10.1063/1.1655067

[36] S.Z. Deng, H.T. Xu, X.G. Zhen, Jun Zhou, Jun Chen, N.S. Xu. *Effect of Temperature on Field Emission Properties from Nanoclusters of Tungsten Oxide on Silicon Carbide* IEEE/CPMT/SEMI. 28th International Electronics Manufacturing Technology Symposium, 07–11 July 2003, IEEE. DOI: 10.1109/IVMC.2003.1223047

[37] Y. Arakawa, A. Yariv. IEEE J. Quant. Electron., **22** (9), 1887 (1986). DOI: 10.1109/JQE.1986.1073185

[38] E.X. Ping, H.X. Jiang. Phys. Rev. B, **40** (17), 11792 (1989). DOI: 10.1103/PhysRevB.40.11792

[39] O. Pinaud. J. Appl. Phys., **92** (4), 1987 (2002). DOI: 10.1063/1.1494127

[40] L. Esaki. IEEE J. Quant. Electron., **22** (9), 1611 (1986). DOI: 10.1109/JQE.1986.1073162

[41] V.F. Elesin. J. Exp. Theor. Phys., **101**, 795 (2005). DOI: 10.1134/1.2149060

[42] V.F. Elesin, Y.V. Kopaev. J. Exp. Theor. Phys., **96**, 1149 (2003). DOI: 10.1134/1.1591227

[43] V.F. Elesin. J. Exp. Theor. Phys., **89**, 377 (1999). DOI: 10.1134/1.558994

[44] V.F. Elesin. J. Exp. Theor. Phys., **85**, 264 (1997). DOI: 10.1134/1.558273

[45] V.F. Elesin. J. Exp. Theor. Phys., **94**, 794 (2002). DOI: 10.1134/1.1477905

[46] V.F. Elesin. J. Exp. Theor. Phys., **117**, 950 (2013). DOI: 10.1134/S1063776113130104

[47] V.F. Elesin. JETP, **118** (6), 951 (2014). DOI: 10.1134/S1063776114060041

[48] M.V. Davidovich. J. Exp. Theor. Phys. Lett., **110** (7), 472 (2019). DOI: 10.1134/S0370274X19190068

[49] M.V. Davidovich, R.K. Yafarov. Tech. Phys., **63** (2), 274 (2018). DOI: 10.1134/S106378421802010X

[50] M.V. Davidovich, R.K. Yafarov. Tech. Phys., **64** (8), 1210 (2019). DOI: 10.21883/JTF.2019.08.47905.402-18

[51] Yu.A. Chaplygin, V.K. Nevolin, V.A. Petukhov. Dokl. Phys., **56**, 1 (2011). DOI: 10.1134/S1028335811010058

[52] J.G. Simmons. J. Appl. Phys., **34**, 1793 (1963). DOI: 10.1063/1.1702682


*Translated by A.Akhtyamov*